# We are IntechOpen, the world's leading publisher of Open Access books Built by scientists, for scientists

**4,800**
Open access books available

**122,000**
International authors and editors

**135M**
Downloads

Our authors are among the

**154**
Countries delivered to

**TOP 1%**
most cited scientists

**12.2%**
Contributors from top 500 universities

CLARIVATE ANALYTICS BOOK CITATION INDEX INDEXED

WEB OF SCIENCE™

Selection of our books indexed in the Book Citation Index in Web of Science™ Core Collection (BKCI)

## Interested in publishing with us?
## Contact book.department@intechopen.com

Numbers displayed above are based on latest data collected.
For more information visit www.intechopen.com

26

# Several Diffractive Optical Elements Fabricated by Femtosecond Laser Pulses Writing Directly

Zhongyi Guo[1,2], Lingling Ran[2,3], Shiliang Qu[1,2] and Shutian Liu[1]
[1]*Department of Physics, Harbin Institute of Technology, Harbin, 150001,*
[2]*Department of optoelectronic science, Harbin Institute of Technology at Weihai, Weihai 264209,*
[3]*College of Electronic Engineering, Heilongjiang University, Harbin 150080, China*

## 1. Introduction

With the developments of the laser technology, femtosecond laser technology is emerging as one of the useful microfabrication tools in recent years for both microfabrication and micro-machining of various multi-functional structures in dielectric materials through multi-photon absorption because of its high-quality and damage-free processing. Many high-quality material processing techniques have been achieved to date by using femtosecond laser pulses with the methods of holographic fabrication [1-8] and direct writing [9-16], such as micro-gratings [1-4], photonic crystals [5-8], waveguide [9] and diffractive optical elements (DOE) [10-16].

In this chapter, we have reported to fabricate several diffractive optical elements (DOEs) on the surface of the metal film or inside transparent silica glass by femtosecond laser pulses writing directly. Firstly, we introduce a method for holographic data storage with the aid of computer-generated hologram (CGH) on the metal film (Au) by femtosecond laser pulses writing directly. Both the simulated and the experimentally restructured object wave show high fidelity to the original object. Then, we introduce a novel method for generating the optical vortex (OV) by fabricating the computer generated hologram (CGH) of the OV inside glass using femtosecond laser directly writing. And the superpositions of the photon orbital angular momentum (OAM) have also been obtained by using a combined computer generated hologram (CCGH). We also give a concrete explanation to the superpositions of the photon OAM. Lastly, we have fabricated volume grating inside silica glass induced by a tightly focused femtosecond laser pulses for improving the first order of the diffractive efficiency. Experimental results show the first order diffractive efficiency (FODE) of the fabricated gratings is depending on the energy of the pulses and the scanning velocity of the laser pulses greatly, and the highest FODE reaches to 30% nearly. The diffraction pattern of the fabricated grating is also numerically simulated and analyzed by using a two dimensional FDTD method and Fresnel Diffraction. The numerical simulated results proved our prediction on the formation of the volume grating is correct which agree well with our experimental results.

## 2. Realizing optical storage by method of computer-generated hologram

Because computer-generated holograms (CGHs) can produce wavefronts with any desired amplitude and phase distributions, they have yielded many applications since Lohmann *et al*. [17, 18] firstly demonstrated it several decades ago, such as optical interconnection [19], spatial filtering [20], three-dimensional display [21, 22], and holographic optical manipulation [23]. Two steps are needed for the production of a Fourier hologram. The first step is to calculate the complex amplitude of the virtual or physical object wave at the hologram plane. The second step involves encoding and production of a transparency.

Here, we introduce a method for holographic data storage with the aid of CGH on the metal film by femtosecond laser pulses writing directly. Firstly, the letter "E" consisted of $64 \times 64$ pixels was selected as the object image depicting in Fig. 1 (a), which was sampled and Fourier transformed by a computer to obtain the discrete complex amplitude distribution. Then, the discrete complex amplitude distribution was encoded by the detour phase method as depicted in Fig. 1 (b), in which the width of the rectangular aperture was set to the half width of the cell; the height of the rectangular aperture was proportional to the modulus of the complex amplitude; and the phase of the complex amplitude was expressed with the distance between the center of the aperture to the center of the cell. The concrete resulted encoded CGH could be found in Fig. 1 (c).

The resulted CGH could be directly written and recorded on the metal film ablated selectively by femtosecond laser pulses with right pulse energy. The experimental setup for the fabrication of the metal film is shown in Fig. 2. A regeneratively amplified Ti:sapphire laser system (Coherent. Co.) was used, which delivered pulses with a duration of 120fs (FWHM), with a center wavelength at 800nm and a repetition rate of 1kHz. The femtosecond laser pulses with proper energy turned by a ND (neutral density) filter is focused on the surface of the metal film with thickness of 130nm deposited on a silica glass substrate by a $50\times$ microscope objective (NA 0.80); the micro-stage with resolution of 0.1 $\mu$m could be controlled by the computer; a shutter system was used to control the ablating area on the surface of the metal film selectively. And the process of the fabrication can be observed by a CCD camera in real-time.

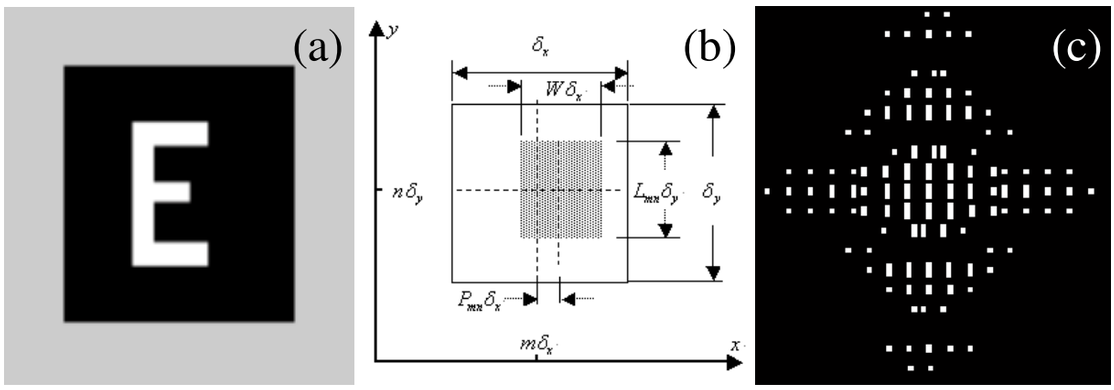


Fig. 1 (a) The object image, (b) The sketch for encoding by the detour phase method, $W = 1/2$, $L_{mn}$ and $P_{mn}$ was proportional to the modulus and the phase of the complex amplitude in the cell (m, n) respectively. (c) The calculated encoded CGH of the object image.

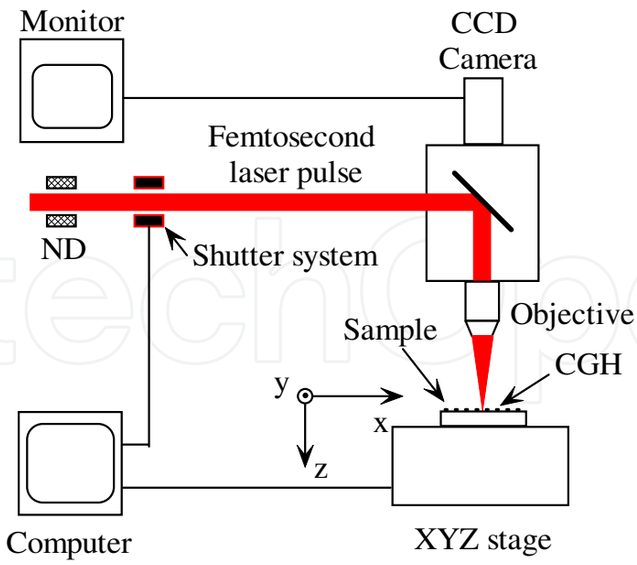


Fig. 2. Experimental scheme of holographic storage on the metal film by femtosecond laser pulses

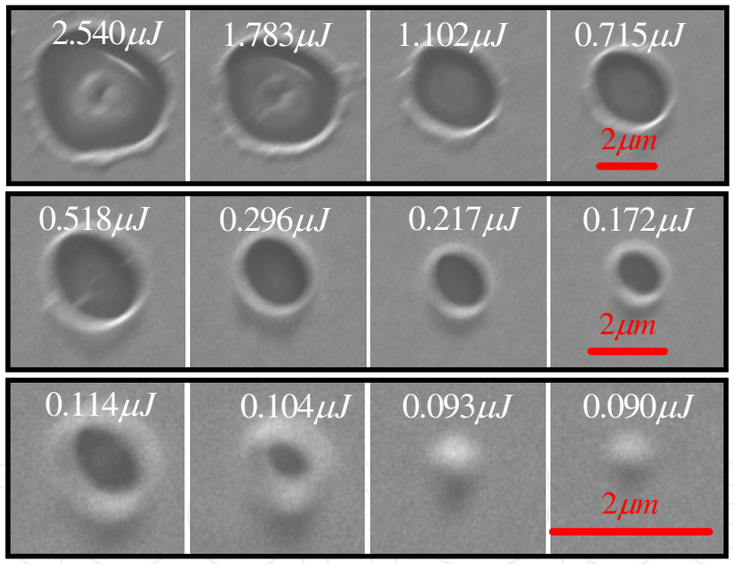


Fig. 3. The hole structures on metal film deposited on glass substrate fabricated by a single femtosecond laser pulse with different pulse energy, all the scale bars are 2 $\mu$m .

Before writing the CGH on the metal film, firstly we need decide the diameters and quality of the ablative spots on the metal film in order to achieve well-defined patterns of CGH. In general, the minimum achievable structure size in laser-processing is determined by the diffraction limit of the optical system and is of the order of the radiation wavelength. However, it is different for the femtosecond laser system, because if we choose the peak laser fluence slightly above the threshold value, only the central part of the beam can modify the material and it becomes possible to produce subwavelength structures [24-25]. The ablated microhole structures could be found in Fig. 3 by scanning electron microscope

(SEM). When the laser pulse energy is set to 2.54$\mu$J, the diameter of the ablated hole for the metal film is about 4.26$\mu$m, and there exist an ablated tiny hole in the substrate. With the decrease of the pulse energy to 1.783$\mu$J, the diameter of the ablated hole for the metal film is also decreased to 4.03$\mu$m. When the pulse energy was changed to 1.1$\mu$J and 0.52$\mu$J, the diameter of the ablated hole can reach to 2.6$\mu$m and 2.2$\mu$m respectively, and the ablated hole in the substrate vanishes either. Although there are not obvious ablated crater on the glass substrate, the diameter is somewhat bigger for fabricating CGH experiments. On the other hand, when the pulse energy was changed to 0.30$\mu$J, the diameter of the ablated hole could reach to 1.1$\mu$m. With energy of the pulse decreasing to 0.217$\mu$J and 0.172$\mu$J, the diameters of the fabricated holes decrease to 800 nm and 600 nm, respectively. When the pulse energy decreases to 0.114$\mu$J and 0.104$\mu$J, the diameter of the fabricated holes decrease to 240 nm and 136 nm respectively, which is less than one third of the wavelength 800 nm and out of the diffraction limit. Especially, when the pulse energy decreases to 0.093$\mu$J and 0.090$\mu$J, there are no ablated holes for the metal film but a nanobump, which could be explained by the T-T model (Two temperatures model) [25]. Although the smaller pulse energy can attain smaller size of the holes and more accurate fabrication in theory, it is difficult to control because of the fluctuations of the energy of the pulses and the thickness of the metal film. Thus, to get a good property of the structured CGH, we choose the pulses energy as 0.30$\mu$J in our experiment.

To record the desired CGH on the metal film, the sample was mounted on a computer-controlled XYZ translation micro-stage with a resolution of 0.1$\mu$m and moved step by step for being ablated selectively by the focused pulses according to the CGH pattern shown in Fig. 1 (c). When the area is black in the hologram, the shutter system will be closed for not being irradiated, while on the contrary, the shutter system will be open for irradiating. The

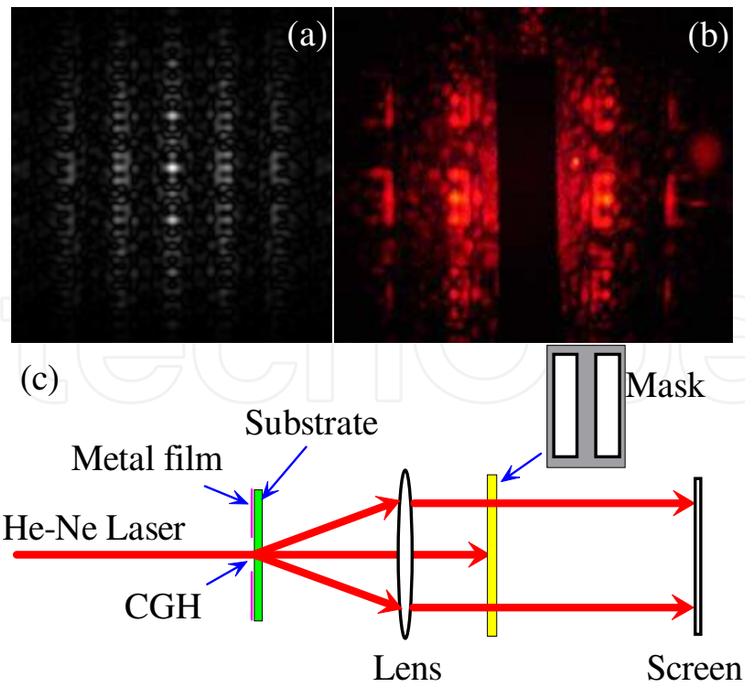


Fig. 4. (a) The simulation of the reconstruction from the CGH; (b) The experimental result; (c) The experimental scheme for the reconstruction of the CGH.

irradiated dots became "transparent" by ablation, while the unexposed dots remained "opaque". The simulated result of reconstruction from the fabricated CGH is given in Fig. 4 (a). In the reconstruction of the CGH, a collimated He-Ne laser beam was used to be incident normally to the CGH on the metal film, as depicted in Fig. 4 (c). The diffraction pattern can be observed in Fig. 4 (b). The letter "E" appears in the +1st order of the diffraction field, while the conjugated image appears in the -1st order of the diffraction field. The result in experiment shows high fidelity to the simulation of the reconstruction. The diffraction efficiency was also measured to be 4.68% by a power meter at the wavelength of 632.8 nm. Here, we defined the diffraction efficiency as a ratio of the intensity of first-order diffraction to that of incident beam.

## 3. Generating optical vortex

Optical vortex (OV) has been paid considerable attentions in the past two decades because of their special characteristics and potential applications [26-28]. OV has been described as a topological point defect (also known as a dislocation) on wavefront and manifest as a "null" within a light beam because the phase at the defect point is undetermined. OV has been applied in many fields, such as optical trapping [23, 29], optical manipulation for MEMS [23], and optical vortex coronagraph [30]. Several methods, such as mode-converters [31], phase mask [32], and computer-generated holograms [13, 28] (CGH), may be used to embed OV into a "background" beam, such as a Gaussian laser beam.

Here, we generate the OV by fabricating the CGHs of the OV inside glass using a near infrared 800 nm femtosecond laser directly writing. The continued and pulsed OV beams have also been reconstructed with both a collimated He–Ne laser beam and the femtosecond laser beam incident to the fabricated CGH, and the first order of the diffraction efficiency could reach to 3.2% nearly.

Nye and Berry [26] have analyzed the phase dislocation within a monochromatic wave in detail in 1974. They have also analyzed a number of optical wavefront dislocations including screw dislocations, edge dislocations and mixed screw-edge dislocations. A monochromatic beam propagating in the z-direction and containing a single vortex transversely centered at the origin (r = 0) can be expressed by the scalar envelope function:

$$u(r,\theta,z) = A_m(r,z)\exp(im\theta)\exp[i\Phi_m(r,z)] \tag{1}$$

Where $u(r,\theta,z)$ is the optical field expressed in cylindrical coordinates with the optical axis aligned along the z axis, $\exp(im\theta)$ is the characteristic expression of the optical vortex, m is a signed integer called the topological charge, $\Phi_m$ is the phase.

To construct a CGH of an OV, we numerically calculate the interferogram of two waves: a planar reference wave and an object wave containing the desired optical vortex. For simplicity, we choose the object wave to be a point vortex of unit charge on an infinite background field of amplitude $C_o$

$$E_o = C_o \exp(im\theta) \tag{2}$$

and a reference wave of amplitude $C_r$, whose wavevector lies in the $(x, z)$ plane, subtending the optical axis, $z$, at the angle $\varphi$, can be expressed as

$$E_r = C_r \exp(-i2\pi x/\Lambda) \tag{3}$$

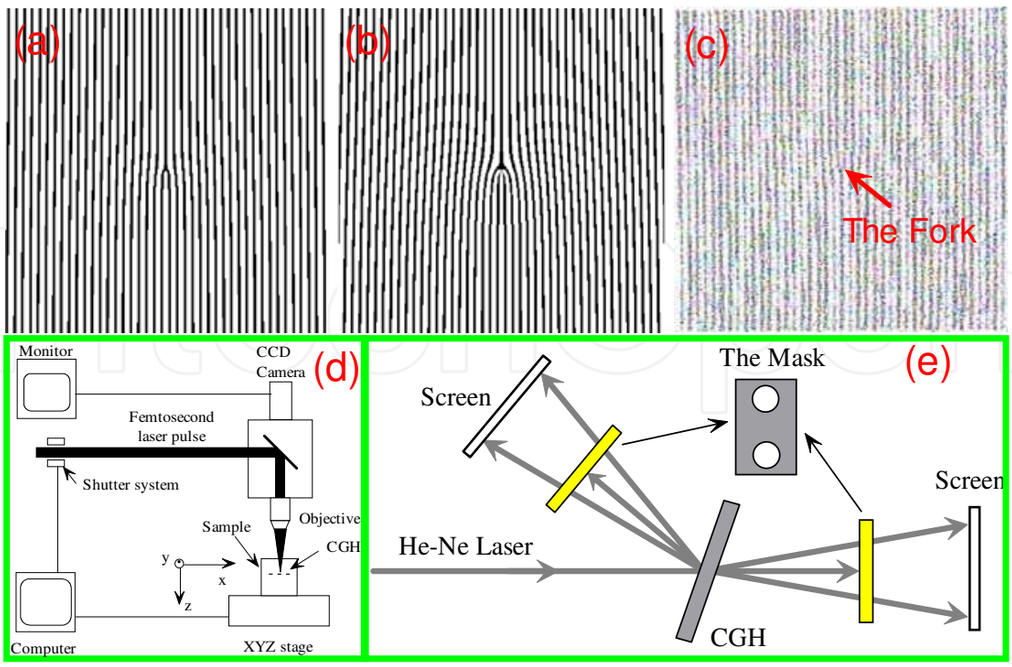


Fig. 5. The CGH interfering between a vortex beam and a planar beam for different topological charge, (a) $m=1$ and (b) $m=3$. (c) Top view of the fabricated CGH. (d) (e) The experimental setup scheme for the fabrication and reconstruction of the CGH respectively.

Where $\Lambda=\lambda/\sin\varphi$ is the spatial period of the plane wave in the transverse plane. The interferogram is given by the intensity of the interfering waves

$$I_{z=0}(x,\theta)=\left|E_o+E_r\right|^2_{z=0}=2C_o\left[1+\cos\left(2\pi x/\Lambda+m\theta\right)\right] \tag{4}$$

Where we set $C_r=C_0$ to achieve unity contrast ($(I_{max}-I_{min})/I_{max}=1$). The resulting interferogram, depicted in Fig. 5 (a) and (b), resembles a sinusoidal intensity diffraction grating. The pattern contains almost parallel lines with a bifurcation at the vortex core.

To record the desired CGH, silica glasses with four planes being polished have been selected as the sample and mounted on a computer-controlled XYZ translation micro-stage with $0.1\mu m$ resolution, which were moved step by step and irradiated by the focused femtosecond laser pulses by a microscope objective lens with a numerical aperture of 0.45 (20X, Nikon.Co.) with proper pulse energy according to the hologram pattern (Fig. 5 (a)) controlled by the PC. The schematic setup is shown in Fig. 5 (d). The irradiated dots would become "black" (opaque) because of microexplosion induced by femtosecond laser pulses inside silica glass while the unirradiated dots remained "white" (transparent). The top view of the fabricated hologram is presented in Fig. 5 (c) according to the CGH depicted in Fig. 5 (a). In general, it is difficult to fabricate microstructure on the surface of the silica glass. The silica glass is transparent at the wavelength of 800 nm because the light frequency is out of the linear absorption range of the silica glass. However, the intensity at focus point would be approximate to 100 TW/cm$^2$. So, high energy fluence within the focal volume would quickly ionize the silicate glass by the combined action of avalanche and multi-photon processes [13, 33].

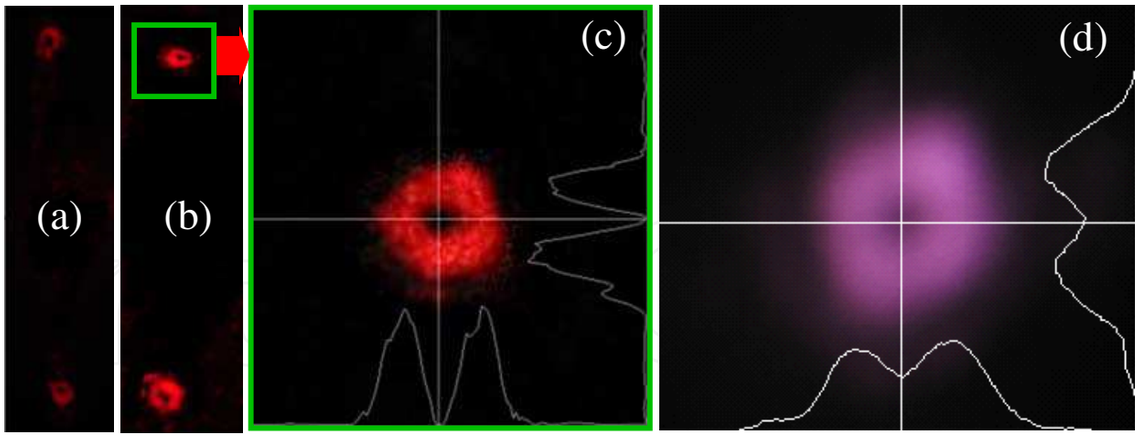


Fig. 6. Diffraction patterns with reconstruction of the CGH shown in Fig. 2. (a) Reflected pattern, (b) Transmitted pattern and (c) The enlarged version of the first-order diffraction of the Transmitted pattern. (d) Reconstructed optical vortex by a femtosecond pulsed laser.

To reconstruct the optical vortex beam from the fabricated CGH, a collimated He–Ne laser beam was incident on the CGH inclined at 30° against the sample, and both the transmission and reflection pattern grating can be realized. In order to get an excellent image, we lay two masks in the diffraction beam path as shown in Fig. 5 (d). Then, the output image could be taken by a digital camera on the screen. Both of the transmission and reflection patterns are shown in Fig. 6 (a) and (b). One vortex of the first-order diffraction in the transmission pattern was taken out for getting an intuitionistic image of the optical vortex in the transverse plane (Fig. 6 (c)). From the result depicted in Fig. 6 (c), we can see that the optical vortex was reconstructed with high fidelity. We have also reconstructed the optical vortex with the femtosecond laser beam with the wave length of 800nm as shown in Fig. 6 (d), which have also shown high fidelity to the optical vortex and been used as a irradiated source for special structures [34].

We have also measured the diffraction efficiency by a power meter at the wavelength of 632.8 nm. Here, we defined the diffraction efficiency as a ratio of the intensity of first-order diffraction to that of incident beam. The efficiency of transmission beams was 3.44%, and that of reflection beams was 1.35%. So, the total efficiency was about 4.79%.

## 4. Realizing the superpositions of the photon OAM by CCGH

As predicted [35] and observed [36], OV beams carry an orbital angular momentum (OAM) distinct from the intrinsic angular momentum of photons associated with their polarizations. This external angular momentum of the photon states is coming from the helical phase structure on the optical wavefront. The OAM of photon states is the reason why they have been suggested for optical data storage [37] and gearing micromachines, such as optical tweezers [23, 29] and optical manipulation for MEMS [23]. The superposition of OAM of photons by Mach-Zehnder interferometer [38-39] has also attracted great attentions because of their potential applications in quantum computation and quantum information processing.

Ordinary beams carry only “spin angular momentum”, encoded in the polarization of light. All possible spin states can be constructed with just two polarization states (vertical and

horizontal, or clockwise and counterclockwise). In 1992, however, Allen [35] showed that OV beams carry a discrete OAM of $m\hbar$ units per photon along their propagation direction because of having an azimuthal phase dependence of the form $\exp(-\mathrm{i}m\theta)$. For the light with OAM, the energy spirals around the beam axis. Therefore there would be OAM transferring to materials while interacting with materials, which can make the particles in the beam spin around the beam axis.

Here, the superpositions of the photon OAM has also been obtained by using a combined computer generated hologram (CCGH) which is fabricated inside the polished silica glass with a near infrared 800 nm femtosecond laser. The CCGH is combined by two special binary CGHs of OV which are recorded by the interference of OV beams with a planar beam simulating on the computer and directly written and recorded inside the glass by femtosecond laser pulses induced microexplosion because of multiphoton absorption. The OV beams with new topological charges can be reconstructed in the diffraction field with a collimated He-Ne laser beam incidence to the fabricated CCGH normally, which reveals the superposition of OAM of photons successfully.

From above, we can obtain two CGHs by choosing topological charges $m=1$ and $m=3$ with the same $\Lambda$ (depicted in Fig. 5 (a) and (b)) for getting the same diffracting angle of the diffracting beams in the same diffracting order. In order to get the CCGH, two CGHs were combined with an orthogonal style by keeping one invariable and the other one rotated to vertical direction (depicted in Fig. 7 (a)).

After getting the binary CCGH, we directly fabricated it inside the silica glass sample with four planes being polished by femtosecond laser pulses writing directly. The same femtosecond laser system was used as the irradiated source, and the schematic setup was

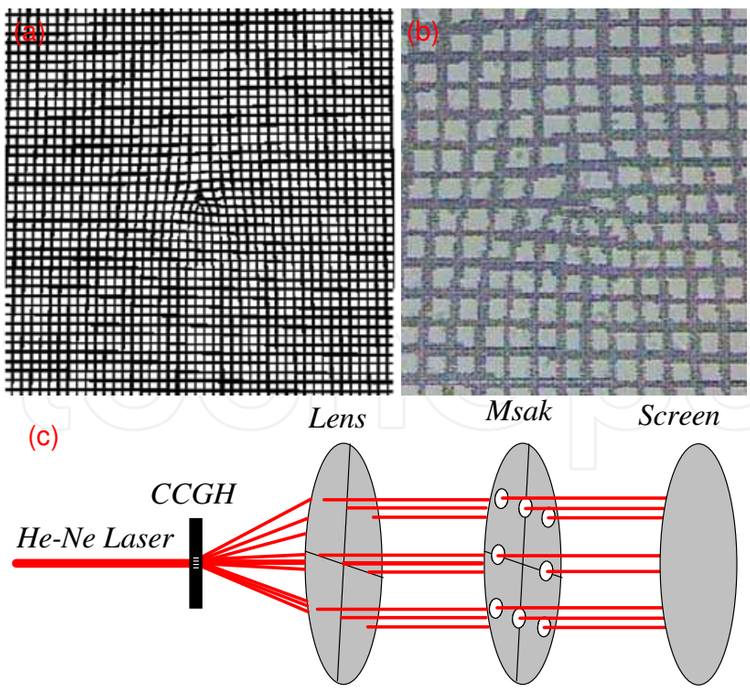


Fig. 7. (a) The CCGH combined with the two CGHs of the optical vortex with topological charges of m=1, m=3 respectively, (b) The top view of the central part of the fabricated CCGH, (c) The experimental setup scheme for the reconstruction of the CCGH.

depicted in Fig. 5 (d). The used pulse energy could be controlled by the ND filter, and the shutter system could control the switch of the femtosecond beam.

To record the desired CCGH, the sample was moved step by step and irradiated selectively by the focused pulses according to the hologram pattern controlled by the PC. When the area is blank in the hologram, the shutter system controlled by the PC will be closed. The irradiated dots became opaque and shown as the "black region" while the unirradiated dots remained transparent as the "white region". The size of the resulted CCGH is $256 \times 256$ , and every pixel in the recorded CCGH is controlled as $2\,\mu m$ . So the scale of the recorded CCGH is $512\mu m \times 512\mu m$ in the silica glass. The top view of the central part of the fabricated hologram under optical microscope is presented in Fig. 7 (b) according to the designed CCGH depicted in Fig. 7 (a).

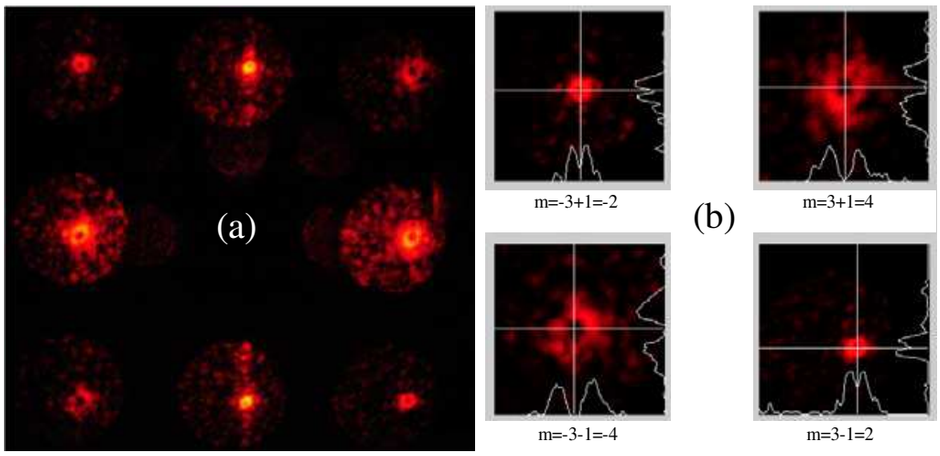


Fig. 8. (a) The diffraction pattern of the fabricated CCGH, (b) The analytical results for the four superposed modes

To reconstruct the optical vortex beams from the fabricated CCGH, a collimated He-Ne laser beam was been incident normally on the CCGH. In order to get an excellent diffraction result, we place a mask with a special aperture array in the diffraction beam path to block out the zero-order diffraction as shown in Fig. 7 (c). Then, the diffraction pattern depicted in Fig. 8 (a) could be taken by a digital camera on the screen. The OV beams with topological charges $m = \pm 1$ and $m = \pm 3$ should be generated in the first order of the diffraction field respectively. However, the OV beams with $m = \pm 2$ and $m = \pm 4$ can also be attained in the first order diffraction modes. We also give an analytical result for the OV beams with new topological charges as shown in Fig. 8 (b), which shows high fidelity to OV beams.

The OVs with new topological charges can be attributed to the superposition of the topological charges between $\pm 1$ orders of the two CGHs. We give a sketch for the explanation of diffraction modes as shown in Fig. 8. We can see that the topological charge is $m = 4$ in the position of the cross between $+1$ order for CGH with $m = 1$ and $+1$ order for CGH with $m = 3$ from the Fig. 9, while the topological charge is $m = -2$ in the position of the cross between $+1$ order for CGH with $m = 1$ and $-1$ order for CGH with $m = 3$.

In order to confirm the theoretical explanation about the superposition of the topological charges, we use another CCGH made by two CGHs with $m = 1$ depicted in Fig. 5(a), and the diffraction pattern is shown in the Fig. 5(b). From the Fig. 5(b), we can find that the

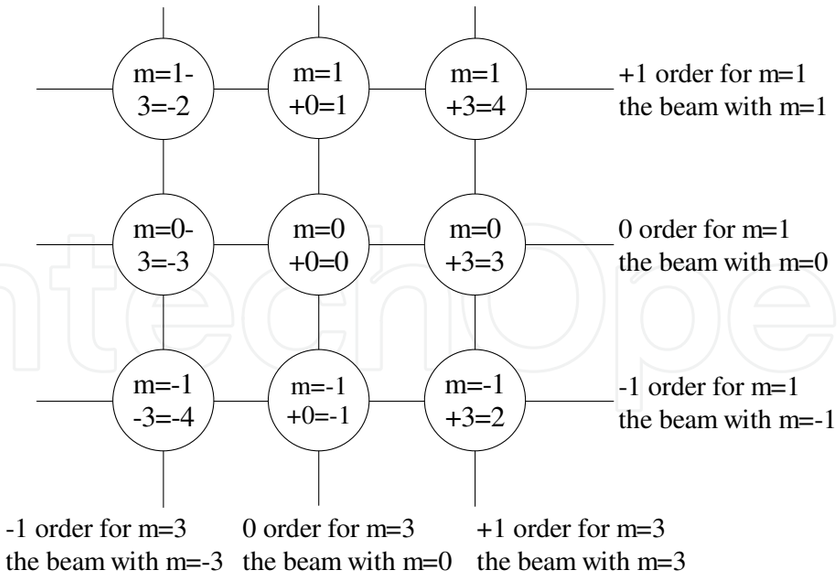


Fig. 9. The sketch for explanation of diffraction mode

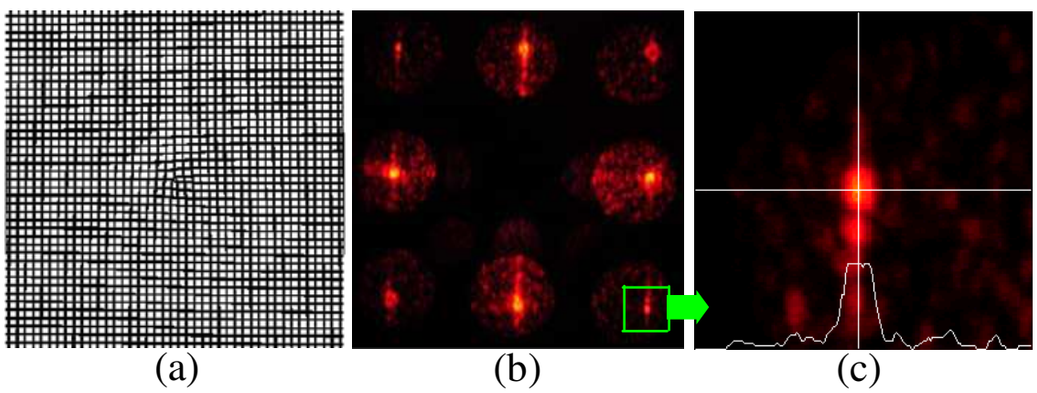


Fig. 10. (a) The CCGH combined by two CGHs with m=1, m=1, (b) The diffraction pattern for the CCGH showed in (a), (c) The enlarged version for the superposed gaussian mode with m=0

diffraction pattern in the position of the cross between the $+1$ order and the $-1$ order has become to a Gauss mode with the topological charge of $m=0$, and the analytical profile of the superposed beam is depicted in Fig. 5(c). It can be seen that our explanation about the superposition of the topological charges is reasonable.

We also measured the diffraction efficiency by a power meter at the wavelength of 632.8 nm. The efficiencies of diffraction beam with $m=\pm1$ and $m=\pm3$ were 2.2% respectively, and those of diffraction beam with $m=\pm2$ and $m=\pm4$ were 1.1% respectively.

The CCGH method would be an effective way to realize the superposition of the photon OAM. It would be significant for the micromachining, optical tweezer, quantum computation and quantum information processing to superpose the diffraction beams with the CCGH combined by two CGHs with the same spatial period $\Lambda$. Because it is much easier to generate the superposition of the OAM of the photons compared to by the methods of Mach-Zehnder interferometer [38, 39].

## 5. Self-assembling volume grating in silica glass

From above experimental results, we can know that the first diffraction efficiencies of the fabricated DOEs are comparatively small. It would be very significant if the diffraction efficiency of these diffractive optical elements could be increased. According to the grating parameter $Q = 2\pi\lambda d \Big/ \left(n\Lambda^2\right)$ defined by Kogelnik [11, 12, 16, 40], where $\Lambda$ is the period of the gratings, $d$ is the thickness of the diffraction grating, $n$ is the refractive index, and $\lambda$ is the wavelength of the incident beam, we can enlarge the thickness or reduce the period of the diffraction grating for obtaining a larger diffraction efficiency. Because of the self-focusing and self-defocusing effects, there would be a line of self-assembly periodic nanovoids generated spontaneously along the propagation direction of the laser beam, when a femtosecond laser beam is focused into transparent glass with proper pulse energy. That is to say the entire length of the void structure and the shapes of the generated voids could be controlled by varying the laser parameters. So far, there have been reported to form a submicrometer-sized void array in borosilicate glass [41], $SrTiO_3$ crystal [42], $Al_2O_3$ crystal [43], CaF2 crystals [44], fused silica glass [45] and so on.

Here, we fabricated volume grating inside silica glass induced by a tightly focused femtosecond laser pulses. The first order diffractive efficiency (FODE) of the fabricated gratings is depending on the energy of the pulses and the scanning velocity of the laser greatly, and the highest FODE reaches to 30% nearly. The diffraction pattern of the fabricated grating is also numerically simulated and analyzed by using a two dimensional FDTD method and Fresnel Diffraction. The numerical simulated results proved our prediction on the formation of the volume grating is correct which agree well with our experiment results.

### 5.1 Experimental results

The schematic illustration of the experimental setup is shown in Fig. 11 (a), which is similar with Fig. 5 (d). The commercially available polishing fused silica glass with size of 8mm×5mm×4mm was mounted on the micro-stage. The laser beam with a diameter of 6mm in Gaussian profile was focused inside the glass sample by a 50X objective lens with numerical aperture of 0.80. And the femtosecond laser beam is focused to 100 $\mu m$ beneath the surface of the sample. The energy of the pulse can be turned by a ND (neutral density) filter. A shutter system was used to control the number of the deposited pulses selectively.

As depicted in Fig. 11 (b-d) , line style structures induced by femtosecond laser pulses consisting of a group of voids and a filamentation could be observed along the incident direction (arrow direction) inside samples. It is observed with the increase of the number of the pulses, the length and the diameter of the induced structure are becoming larger and larger and the void group is becoming more regular (see Fig. 11 (b)). Similarly, with the increase of the pulse energy, the length of the line structures induced by both single pulse (see Fig. 11 (c)) and the double pulses (see Fig. 11 (d)) are also becoming longer, which implies with the decrease of the scanning speed (more laser pulses irradiating in a certain spot) and the increase of the pulse energy, the length of the fabricated line structure would be increased. It is notable to mention that when the pulse energy is decreased to 3.80$\mu$J for the single pulse interacting, the voids almost disappear, with a long sharp filamentation left, as is depicted in Fig. 11. (c). The formation of the filamentation in the silica glass sample is one of the most fundamental nonlinear optical phenomena and results from the dynamic

balance between self-focusing arising from an increase in the refractive index and self-defocusing arising from diffraction or plasma formation [46-47].

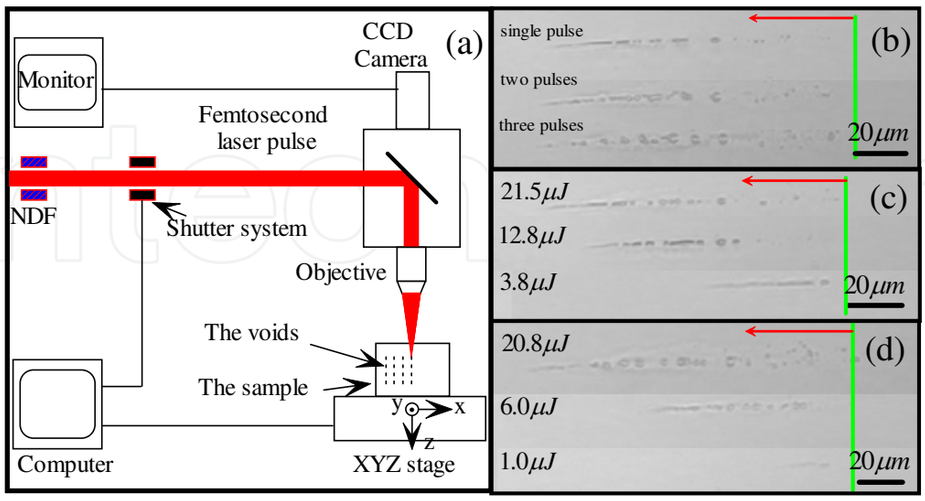


Fig. 11. (a) The sketch of the experimental setup for the generation of periodic voids, Side view of the voids array induced in silica glass by femtosecond laser pulses, (b) Different number of with pulse energy of 20$\mu J$, (c) Single pulse with different energies, (d) Double pulses with different energies. The scale bars in the Figure are 20$\mu m$. The arrows show the direction of the pulses propagation, and the lop lines express the focus place

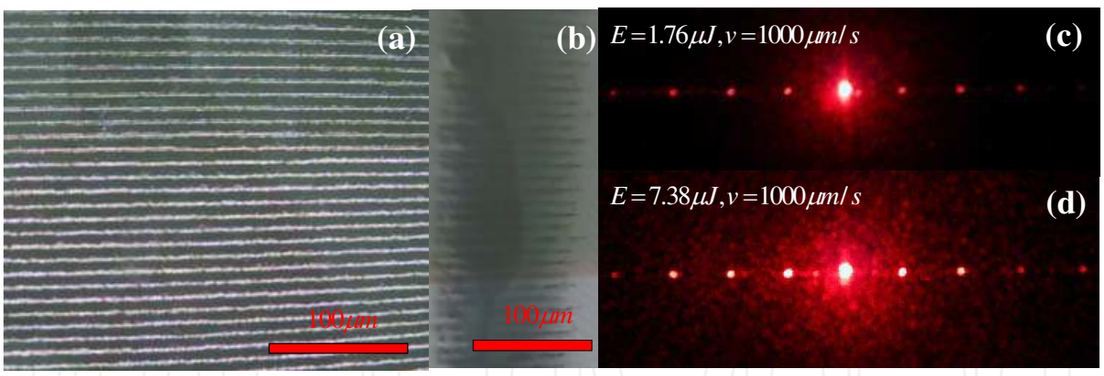


Fig. 12. the fabricated grating: (a) top view, (b) side view; diffraction pattern of the grating obtained under different conditions: (c) E=1.76$\mu J$, v=1000$\mu m/s$, (d) E=7.38$\mu J$, v=1000$\mu m/s$

A series of grating could be fabricated in the silica glass sample by moving the computer-controlled XYZ translation micro-stage at different scanning speeds and different pulse energies. One of the typical fabricated grating is shown in Fig. 12 (a) and (b) with the pulse energy and the moving speed of the stage of E=3.520$\mu J$ and v=500$\mu m/s$ respectively. The period of the fabricated grating is set to 20$\mu m$. From Fig. 12 (b), we can observe that the depth of the grating is reaching to 120$\mu m$ nearly, which is six times of the periods, so we called it volume gratings. The diffraction pattern of the fabricated grating could be obtained by a collimated He-Ne laser beam normally incident on the fabricated grating, and two typical diffraction patterns are depicted in Fig. 12 (c) and (d) by keeping the scanning speed

at v=1000$\mu m/s$ but different pulse energy E=1.176$\mu J$ and E=7.380$\mu J$ respectively. It is apparent that the first diffraction efficiency of the fabricated grating by E=7.380$\mu J$ is larger than that of E=1.176$\mu J$, which shows the first diffraction efficiency of the fabricated grating is depending upon the pulse energies greatly.

We also measure the transmittance efficiency and diffraction efficiency of the fabricated gratings by laying a power meter at the wavelength of 632.8nm behind the sample for detecting the diffractive He-Ne laser. Here, we defined the transmittance efficiency (TE) to be the ratio between the intensity of whole transmittance and that of incident beam. The variation tendency of the transmittance efficiency with the different pulse of energy and scanning velocity is shown in Fig. 13 (a). We found that the transmittance efficiency decreases for higher pulse energy and slower scanning speed. It can be explained by the fact that the absorption and scatterance are enhanced because of stronger microexplosion and the more generation of color centers. We also defined the first order diffraction efficiency (FODE) and normalized first order diffraction efficiency (NFODE) to be the ratio of the intensity of the first-order diffraction to the incident intensity and the transmitted intensity respectively. And the corresponding variation tendencies are shown in Fig. 13 (b) and (c). With the increase of the pulse energy, the FODE would enlarge to a maximum firstly, and then decrease gradually depicted in Fig. 13 (b). However, NFODE nearly increases all the time as shown in Fig. 13 (c) expect for situations with too large energies.

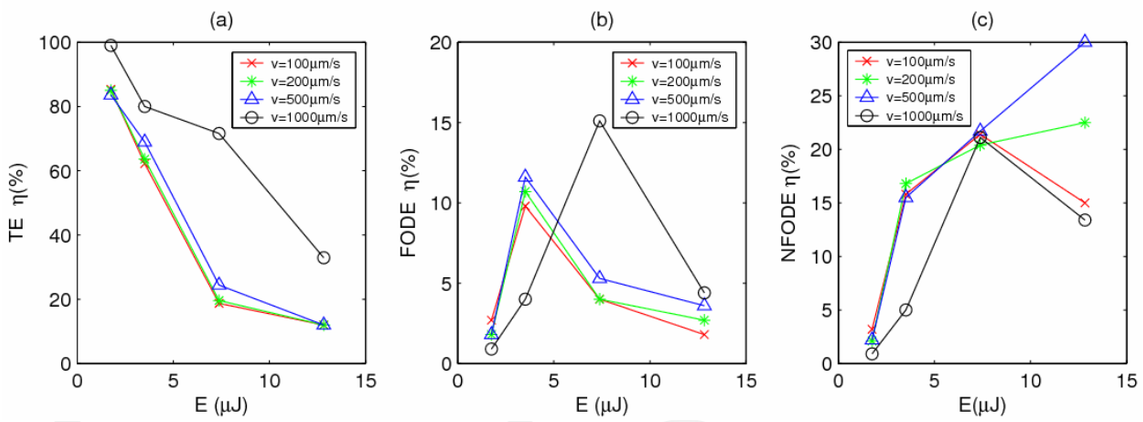


Fig. 13. (a) Variational tendency of the transmittance efficiency(TE) with the different pulse of energy and scanning velocity, (b) Variational tendency of the first order diffraction efficiency(FODE) with the different pulse of energy and scanning velocity, (c) Variational tendency of the normalized first order diffraction efficiency(NFODE) with the different pulse of energy and scanning velocity.

Now we give a physical description of the phenomenon observed above: With the increase of the pulse energy, the depth of the fabricated gratings would be increased, so does the first order diffraction according to Kogelnik's equation [13]. However, the absorption and scatterance are also enhanced at the same time. When the former is dominated, the FODE would be increasing; while the posterior is dominated, the FODE would be decreasing, as shown in Fig. 13 (b). On the other hand, if we neglect the influence of the absorption and scatterance, the NFODE should be always increasing as is depicted in Fig. 13 (c). For different scanning speed at the pulse energy of 1.760$\mu J$, it is observed that the FODE decreases with increasing scanning speed, and the maximum is only 3.2% for v=100$\mu m/s$.

However, when the pulse energy increase to 3.520$\mu J$, the maximum of the FODE reaches to 11.6% for v=500$\mu m/s$, and the FODE for circumstance of v=100$\mu m/s$ and v=200$\mu m/s$ are comparatively small compared to v=500$\mu m/s$. For the pulse energy of 7.380$\mu J$, the biggest diffraction efficiency reaches to 15.1% for v=1000$\mu m/s$, but the others decrease to a lower level compared to that of E=3.520$\mu J$. Going on increasing the pulse energy to 12.83$\mu J$, all of the FODE decrease to a relative lower level compared to E=7.380$\mu J$.

We deem that when the pulse energy is 1.760$\mu J$, the induced microexplosion and the darkening region is comparatively small. When the scanning speed is slow, the fabricated grating is thicker than that for large scanning speed, so the FODE is larger. While the pulse energy reaches to 3.520$\mu J$, the depth of the gratings would be bigger, so the FODE would become bigger than the former. The microexplosion and the darkening region would also increase, and the slower the bigger, so the FODE for v=100$\mu m/s$ is smaller than that for v=500$\mu m/s$ and v=200$\mu m/s$. For v=1000$\mu m/s$, the resulted grating is not so compacted compared with other scanning speed, so the FODE is smaller. However, when the pulse energy reaches to 7.380$\mu J$, the resulted gratings could be compacted enough, so the FODE reaches maximum too. But for v=500$\mu m/s$, v=200$\mu m/s$, and v=100$\mu m/s$, the FODE is decreasing at E=7.380$\mu J$ because of the enhancement of the microexplosion and the darkening region. For pulse energy of 12.83$\mu J$, resulted gratings is too compacted, and the absorption and scatterance dominate, so all of the FODE is decreased to a lower level. Moreover, the order of the FODE is in a reverse order compared to that of E=1.760$\mu J$, just because of the different dominant mechanism for lower and higher energy.

### 5.2 Simulated results

In order to verify our explanation on experimental results, we simulate the diffraction process of the induced gratings without regard to the optical absorption by the combined methods of two dimensional FDTD and Fresnel diffraction as shown in Fig. 14 (a-c). The scale of the simulation districts is chosen to be $h_x = 200\mu m$ and $h_z = 80\mu m$, and assume the sample is uniform along the direction of Y axes. The grating period is set as $d_x = 20\mu m$ according to our experimental reality, and the refractive indexes of silica glass and the filamentations are $n_s = 1.5$ and $n_f = n_0 + \delta n$ respectively, where $\delta n$ is the refractive index change (RIC) induced by the laser. The refractive index of the background (air) is $n_b = 1.0$. According to our experimental results as depicted in Fig. 11 (b-d), the filamentations could be simplified as composite regions combined by a rectangle and followed by a triangle (see Fig. 14 (b)), and the width of the rectangle region is $d_{rect}$. In our simulation, the sample is divided into four regions labelled A, B, C and D respectively, and the length (along Z axes) of region A, B are set as $h_A = 5\mu m$ and $h_B = 10\mu m$ respectively. We could change the length of region C ($h_C$), the refractive index variation $\delta n$ and the width of the rectangle region $d_{rect}$, so as to match different conditions in our experiment. We use a Gauss form continuous source in front of the sample with a twist $\omega_0 = 40\mu m$ and wavelength $\lambda_0 = 0.8\mu m$. The position of the source waist is marked with green line in Fig. 14 (b).

To obtain the far field diffraction, we extract the amplitude and phase distribution of the electric field in the plane $(x, y)$ behind the silicate sample to be $E(x) = A(x)e^{i\phi(x)}$, and assume the scale of the sample in the third dimension to be constant. Then the diffraction pattern of the far field in the $(x', y')$ plane can be solved using the Fresnel Diffraction Integral as below:

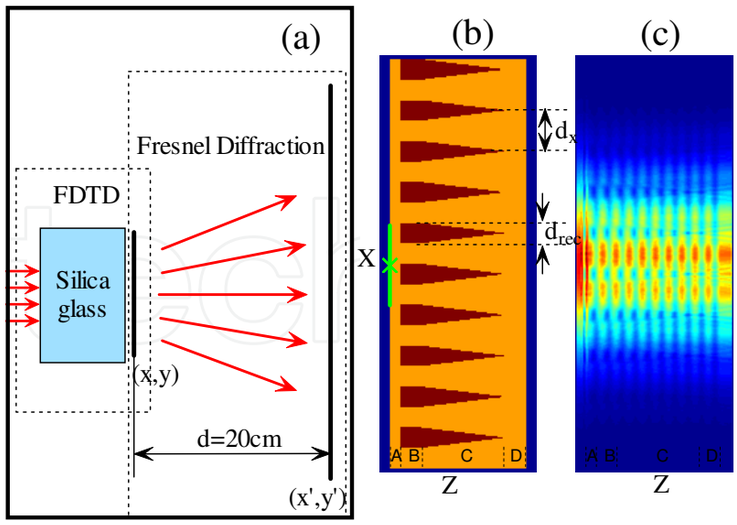


Fig. 14. (a) A simple sketch of our numerical method, (b) A typical example of the distribution of the amplitude of the electric field inside the sample. (c) Distribution of the amplitude of the Electric filed in the silicate glass sample.

$$E(x') = \frac{C}{j\lambda}\int_{-\infty}^{+\infty} E(x)\frac{\exp(ikr)}{r}\frac{\cos\theta + 1}{2}dx \tag{5}$$

Where $r = \sqrt{d^2 + (x - x')^2}$, $\theta = \arccos(d / r)$, $k$ is the wave-number, $C$ is an constant introduced by the integration along the third dimension. The distance between the two planes is fixed to be $d = 20\text{cm}$, which is in consistent with our experiment. And we observe the distribution of the electric field in the $(x', y')$ plane along the $x'$ axis.

The numerical simulated results are shown in Fig. 15. After more than 20000 iterations, we could attain stationary distribution of the electric amplitude inside the silicate glass sample as depicted in Fig. 14 (c) (at $h_C = 40\mu\text{m}, \delta n = 0.002, d_{rec} = 10\mu\text{m}$). The far field diffraction patterns of the given volume grating at which $d_{rec} = 10\mu\text{m}, \delta n = 0.005$ with different depths( $h_c = 10, 20, 40\mu m$ ) are depicted in Fig. 15 (a), which shows that with the increase of the depth of the grating, the diffraction efficiency is increasing, which verify our former physical explanation and agree with our experimental results very well as depicted in Fig. 13 (c).

With the increase of the pulse energy or decrease of the scanning speed, the fabricated lines' width ( $d_{rec}$ ) of the induced grating would increase obviously as depicted in Fig. 11 (b-d). So we also give a numerical simulation on the far field diffraction patterns of the volume grating by keeping $h_c = 20\mu\text{m}$ and $\delta n = 0.005$ but with different line widths ( $d_{rec} = 15, 10, 5\mu m$ ) are depicted in Fig. 15 (b), which shows that with the increase of the line width ( $d_{rec}$ ), the first order diffraction efficiency is increasing. In other words, increasing the incident pulse energy (leading to the increase of the line width and the depth of the induced grating) would enhance the FODE if we can take no account of the absorption.

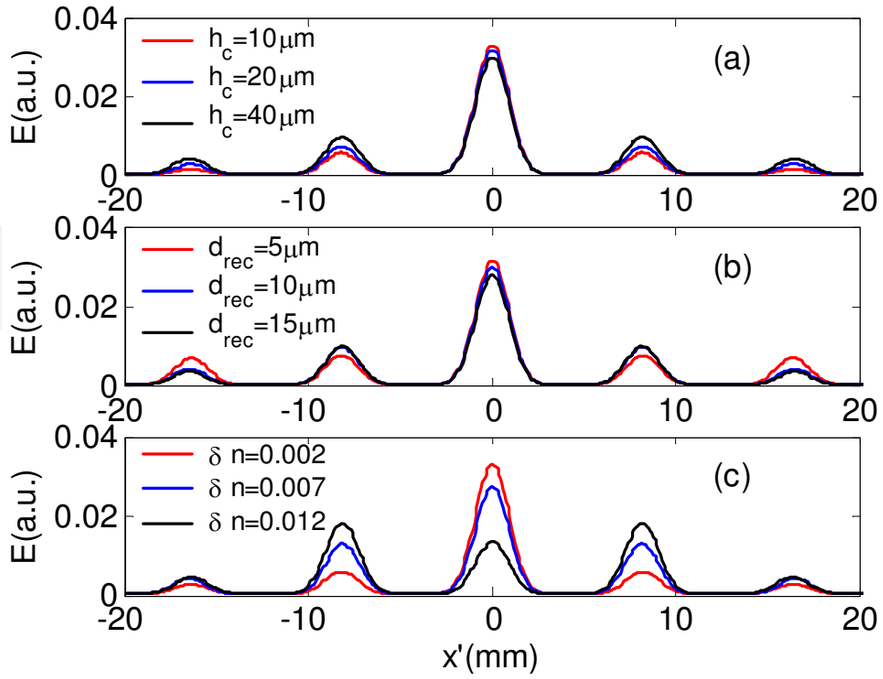


Fig. 15. The far field diffraction of the distribution of Electric filed along the $x'$ direction, (a) $h_{rec} = 10\mu m, \delta n = 0.002$ and the three curves correspond to different depths of the induced gratings: $h_c$ = 10(red), 20(blue) and 40 μm (black) respectively; (b) $h_c = 10\mu m, \delta n = 0.002$ and the three curves correspond to different width of the filaments: $d_{rec}$ = 15(red), 10(blue) and 5 μm (black) respectively; (c) $d_{rec} = 10\mu m, h_c = 40\mu m$ and the three curves correspond to different variations of the refractive index: $\delta n = 0.007$ (red), 0.005 (blue) and 0.012(black) respectively.

We also simulated FODEs depending on the different RIC ( $\delta n = 0.002, 0.007, .0012$ ) by remaining $d_{rec} = 10\mu m, h_c = 40\mu m$ . From the simulated result as shown in Fig. 15 (c), we can observe that the RIC would affect the FODE strongly. Especially, for $\delta n = 0.012$ , the FODE is higher than the zero order diffraction efficiency (ZODE) for the normally incident beam. In fact, in our simulation if we further enlarge the RIC, the ZODE would be minished correspondingly. It is possible that the ZODE minish to zero absolutely at a certain RIC that relates to the depth of the grating ( $h_c$ ). That is to say the energy of the zero order diffraction could transfer to the first and higher order diffraction. Therefore, if we can accurately control the RIC and $h_c$ inside the glass sample induced by femtosecond laser, we could control the diffraction pattern very well.

## 6. Conclusion

In conclusion, optical information has been stored on the metal film by femtosecond laser pulses with the aid of the computer-generated hologram (CGH) encoded by the detour phase method. Furthermore, the object wave has been reconstructed by using a collimated He-Ne laser beam in a proper way, and the result shows a high fidelity to the original object.

The CGH of the OV has been fabricated inside glass by the femtosecond laser pulses. And we realized the restructured optical vortex beam of both the transmission and reflection pattern with high fidelity using a collimated He–Ne laser beam. We have realized the superposition of the OAM of photons with CCGH of OVs. The CCGH was formed by combining two CGHs of OVs in a special way and directly written inside glass by femtosecond laser pulses induced microexplosion. The OV beams with different photon OAM can be generated from different topological charges carried by the diffraction beams from the CCGH. Theoretical analysis and experimental demonstrations have been given to explain the generations of the superposition of the OAM. The efficiencies of the first order diffraction waves have been measured to be about 6.6% in total.

In order to enhance the first order diffraction efficiency, we have researched the way to fabricating the volume grating inside silica glass by tightly focused femtosecond laser pulses. The femtosecond pulses induced multiple microexplosion and the self-focusing and self-defocusing effects in the transparent materials have been considered as the reasons for the formation of volume grating. The first order diffraction efficiency of the induced grating is measured by a collimated He-Ne laser and the highest NFODE reaches to 30% nearly. We also have constructed a grating mode and attained the simulated results by using a two dimensional FDTD method and Fresnel Diffraction. The numerical simulated results verified our physical viewpoint on the formation of the volume grating is correct which agree well with our experiment results.

## 7. Acknowledgment

This work was supported by the National Science Foundation of China (NSFC: 10904027), the China Postdoctoral Science Foundation (AUGA41001348) and the Heilongjiang Province Postdoctoral Science Foundation (AUGA1100074), and development program for outstanding young teachers in Harbin Institute of Technology, HITQNJS. 2009. 033.

## 8. Reference

[1] S. Qu, J. Qiu, C. Zhao, X. Jiang, H. Zeng, C. Zhu, and K. Hirao, "Metal nanoparticle precipitation in periodic arrays in $Au_2O$-doped glass by two interfered femtosecond laser pulses," *Appl. Phys. Lett.* 84, 2046-2048, (2005).

[2] Y. Han, S. Qu, Q. Wang, Z. Guo, and X. Chen, Controllable grating fabrication by three interfering replicas of single femtosecond laser pulse, Chinese physics B, 18, 5331, (2009).

[3] S. Qu, C. Zhao, Q. Zhao, J. Qiu, C. Zhu, and K. Hirao, One-off writing of multimicrogratings on glass by two interfered femtosecond laser pulses, Opt. Lett. 29, 2058 (2004).

[4] Z. Guo, S. Qu, L. Ran, and S. Liu, Modulation grating achieved by two interfered femtosecond laser pulses on the surface of the silica glass, Appl. Surf. Sci., 253, 8581, (2007).

[5] T. Kondo, S. Matsuo, S. Juodkazis, V. Mizeikis, and H. Misawa, "Multiphoton fabrication of periodic structures by multibeam interference of femtosecond pulses," *Appl.Phys.Lett.* 82 (2003) 2758-2760.

[6] Z. Guo, L. Ran, Y. Han, S. Qu, and S. Liu, "The formation of novel two-dimensional periodic microstructures by a single shot of three interfered femtosecond laser pulses on the surface of the silica glass", *Opt. Lett.* 33 (2008) 2383.
[7] Z. Guo, S. Qu, Y. Han, and S. Liu, Multi-photon fabrication of two-dimensional periodic structure by three interfered femtosecond laser pulses on the surface of the silica glass, Optics Communications, 280, 23-26, (2007).
[8] J. Si, Z. Meng, S. Kanehira, J. Qiu, B. Hua and K. Hirao, "Multiphoton-induced periodic microstructures inside bulk azodye-doped polymers by multibeam laser interference", *Chem. Phys. Lett.* 399 (2004) 276-279.
[9] C. Schaffer, A. Brodeur, J. García, and E. Mazur, "Micromachining bulk glass by use of femtosecond laser pulses with nanojoule energy," Opt. Lett. 26, 93-95 (2001)
[10] Y. Li, Y. Dou, R. An, H. Yang, and Q. Gong,, "Permanent computer-generated holograms embedded in glass by femtosecond laser pulses," *Opt. Express,* 13 (2005) 2433-2438.
[11] Q. Zhao, J. Qiu, X. Jiang, E. Dai, C. Zhou, and C. Zhu, "Direct writing computer-generated holograms on metal film by an infrared femtosecond laser," *Opt. Express,* 13 (2005) 2089-2092.
[12] Z. Guo, S. Qu, Z. Sun, and S. Liu, "Superposition of orbit angular momentum of photons by combined computer-generated hologram fabricated in silica glass with femtosecond laser pulses", *Chin. Phys. B.* 17 (2008) 4199.
[13] Z. Guo, S. Qu, S. Liu, Generating optical vortex with computer-generated hologram fabricated inside glass by femtosecond laser pulses, Optics Communications, 273, 2007, 286-289.
[14] Z. Guo, H. Wang, Z. Liu, S. Qu, J. Dai, and S. Liu, Realization of holographic storage on metal film by femtosecond laser pulses micromachining, Journal of Nonlinear Optical Physics and Materials, 18(4), 2009, 617-623.
[15] Z. Guo, W. Ding, S. Qu, J. Dai, and S. Liu, Self-assembled volume grating in silica glass induced by a tightly focused femtosecond laser pulses, Journal of Nonlinear Optical Physics and Materials, 18(4), 2009, 625-632.
[16] K. Zhou, Z. Guo, W. Ding, and S. Liu, Analysis on volume grating induced by femotosecond laser pulses, Opt. Express 18(13), 2010, 13640-13646.
[17] A. W. Lohmann and D. P. Paris, "Binary Fraunhofer holograms generated by computer," *Appl. Opt.* 5 (1967) 1739.
[18] B. R. Brown and A. W. Lohmann, "Computer-generated binary holograms," *IBM J. Res. Develop.* 13 (1969) 160.
[19] M. R. Feldman and C. C. Guest, "Computer generated holographic optical elements for optical interconnection of very large scale integrated circuits," *Appl. Opt.* 26 (1987) 4377.
[20] B. R. Brown and A. W. Lohmann, "Complex spatial filtering with binary masks," *Appl. Opt.* 5 (1966) 967.
[21] O. Bryngdahl and F. Wyrowski, "Digital holography - computer-generated holograms" in *Progress in Optics*, E. Wolf, ed. (North-Holland, Amsterdam, 1990), 28, pp.1–86.
[22] D. Abookasis and J. Rosen, "Computer-generated holograms of three-dimensional objects synthesized from their multiple angular viewpoints," *J. Opt. Soc. Am. A,* 20 (2003) 1537.
[23] D. G. Grier, "A revolution in optical manipulation," *Nature* 424 (2003) 810.

[24] Y. Li，W. Watanabe, K. Yamada, T. Shinagawa, K. Itoh, J. Nishii, and Y. Jiang "Holographic fabrication of multiple layers of grating inside soda–lime glass with femtosecond laser pulses". *Appl.Phys.Lett,* 80 (2002) 1508.
[25] J. Koch, F. Korte, T. Bauer, C. Fallnich, A. Ostendorf, B. Chichkov. Nanotexturing of Gold Films by Femtosecond Laser-induced Melt Dynamics. Appl. Phys. A. 2005, 81:325–328.
[26] J. F. Nye and M. V. Berry, 1974 Proc. R. Soc. A. 336 165-190.
[27] G. A. Turnbull, D. A. Robertson, G. M. Smith, L. Allen, and M. Padgett, 1996 Opt. Comm. 127 183-188.
[28] V. Y. Bazhenov, M. V. Vasnetsov, and M. S. Soskin, 1990 Pis'ma Zh. Eksp. Teor. Fiz. 52, 1037-1039 [1990 JETP Lett. 52 429-431].
[29] M. Dienerowitz, M. Mazilu, P. Reece, T. Krauss, and K. Dholakia, "Optical vortex trap for resonant confinement of metal nanoparticles," Opt. Express 16, 4991-4999 (2008).
[30] G. Foo, D. Palacios, and G. Swartzlander, Jr., "Optical vortex coronagraph," Opt. Lett. 30, 3308-3310 (2005)
[31] M. Beijersbergen, L. Allen, H. van der Veen and J. Woerdman, Astigmatic laser mode converters and transfer of orbital angular momentum, *Opt. Commun.* 96 (1993), 123.
[32] G. Turnbull, D. Robertson, G. Smith, L. Allen and M. Padgett, The generation of free-space Laguerre-Gaussian modes at millimetre-wave frequencies by use of a spiral phaseplate, *Opt. Commun.* 127 (1996), 183.
[33] S. Juodkazis, H. Misawa, T. Hashimoto, E. Gamaly, and B. Luther-Davies, Laser-induced microexplosion confined in a bulk of silica: Formation of nanovoids, *Appl. Phys. Lett.* **88** (2006), 201909
[34] L. Ran, and S. Qu, Self-assembled volume vortex grating induced by femtosecond laser pulses in glass, *Current Applied Physics*, 9, 2009, 1210-1212.
[35] L. Allen, M. Beijersbergen, Orbital angular momentum of light and the transformation of Laguerre-Gaussian laser modes, Phys. Rev. A, 45, 1992, 8185-8189.
[36] H. He, M. Friese, and N. Heckenberg, Direct Observation of Transfer of Angular Momentum to Absorptive Particles from a Laser Beam with a Phase Singularity, Phys. Rev. Lett. 75, 1995, 826-829.
[37] G. Gibson, J. Courtial, M. Padgett, M. Vasnetsov, V. Pas'ko, S. Barnett, and S. Franke-Arnold, "Free-space information transfer using light beams carrying orbital angular momentum," Opt. Express 12, 5448-5456 (2004).
[38] J. Leach, and J. Courtial, Interferometric Methods to Measure Orbital and Spin, or the Total Angular Momentum of a Single Photon, Phys. Rev. Lett. 92, 2004, 013601.
[39] W. Jiang, Q. Chen, Y. Zhang, and G. Guo, Computation of topological charges of optical vortices via nondegenerate four-wave mixing, Phys. Rev. A, 74, 2006, 043811.
[40] H. Kogelnik, "Coupled wave theory for thick hologram gratings," *Bell Syst. Tech. J.* 48 (1969) 2909-2947.
[41] S. Kanehira, J. H. Si, J. R. Qiu, K. Fujita, and K. Hirao, Periodic nanovoid structures via femtosecond laser irradiation, *Nano Lett.* 5 (2005) 1591.
[42] Juan Song, Xinshun Wang, Jian Xu, Haiyi Sun, Zhizhan Xu, and Jianrong Qiu, "Microstructures induced in the bulk of SrTiO3 crystal by a femtosecond laser," *Opt. Express.* 15 (2007) 2341-2347.

[43] Xiao Hu, Juan Song, Qinling Zhou, Luyun Yang, Xiaodan Wang, Congshan Zhu, and Jianrong Qiu, "Self-formation of void array in $Al_2O_3$ crystal by femtosecond laser irradiation," *Chin. Opt. Lett.* 6 (2008) 388-390.

[44] X. Hu , B. Qian, P. Zhang, X. Wang, L. Su, J. Qiu, C. Zhu, Self-organized microvoid array perpendicular to the femtosecond laser beam in $CaF_2$ crystals, Laser Phys Lett, 5(5) (2008) 394.

[45] E. Toratani, M. Kamata, and M. Obara, Self-fabrication of void array in fused silica by femtosecond laser processing, *Appl. Phys. Lett.* 87 (2005) 171103.

[46] J. Song, X. Wang, X. Hu, Y. Dai, J. Qiu, Y. Cheng and Z. Xu, Formation mechanism of self-organized voids in dielectrics induced by tightly focused femtosecond laser pulses, *Appl. Phys. Lett.* 84 (2008) 092904.

[47] Brodeur, F. Ilkov and S. Chin, Beam filamentation and the white light continuum divergence, *Opt. Comm.* 96 (1996) 193-198.

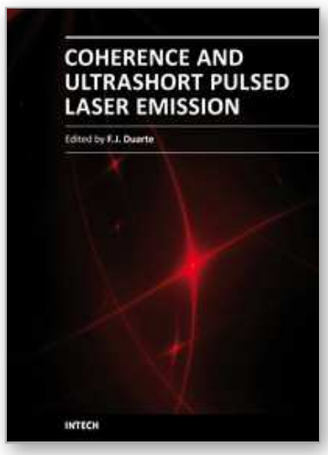


**Coherence and Ultrashort Pulse Laser Emission**
Edited by Dr. F. J. Duarte

ISBN 978-953-307-242-5
Hard cover, 688 pages
**Publisher** InTech
**Published online** 30, November, 2010
**Published in print edition** November, 2010

In this volume, recent contributions on coherence provide a useful perspective on the diversity of various coherent sources of emission and coherent related phenomena of current interest. These papers provide a preamble for a larger collection of contributions on ultrashort pulse laser generation and ultrashort pulse laser phenomena. Papers on ultrashort pulse phenomena include works on few cycle pulses, high-power generation, propagation in various media, to various applications of current interest. Undoubtedly, Coherence and Ultrashort Pulse Emission offers a rich and practical perspective on this rapidly evolving field.



**InTech Europe**
University Campus STeP Ri
Slavka Krautzeka 83/A
51000 Rijeka, Croatia
Phone: +385 (51) 770 447
Fax: +385 (51) 686 166
www.intechopen.com

**InTech China**
Unit 405, Office Block, Hotel Equatorial Shanghai
No.65, Yan An Road (West), Shanghai, 200040, China
中国上海市延安西路65号上海国际贵都大饭店办公楼405单元
Phone: +86-21-62489820
Fax: +86-21-62489821

IntechOpen